Automated image analysis techniques for cardiovascular magnetic resonance imaging

Geest, R.J. van der

CHAPTER

2

Quantification in cardiac MRI

This chapter was adapted from:

Quantification in cardiac MRI
Rob J. van der Geest, Johan H.C. Reiber
Journal of Magnetic Resonance Imaging 1999, Volume 10, Pages 602-608.

Quantification of global and regional ventricular function in cardiac magnetic resonance imaging
Rob J. van der Geest, Boudewijn P.F. Lelieveldt, Johan H.C. Reiber
Topics in Magnetic Resonance Imaging 2000
Volume 11, Issue 6, Pages 348-358.

Quantification in cardiac magnetic resonance imaging and computed tomography
Rob J. van der Geest, Boudewijn P.F. Lelieveldt, Johan H.C. Reiber
In: Higgins CB, de Roos A, eds. MRI and CT of the cardiovascular system (second edition). Philadelphia, PN, 2006:91-106.

2.1 Introduction

Magnetic resonance imaging (MRI) has become an indispensable imaging modality for the evaluation of the cardiac system. MRI stand outs as is provides unique capabilities for studying many aspects of cardiac anatomy, function, perfusion and viability in a single imaging session. Volumetric measurement of the ventricular cavities and myocardium can be performed at high accuracy and precision as have been demonstrated in many experimental and clinical research studies. The 3D-nature of cardiovascular MRI also provides detailed information of the cardiac system at a regional level. Among others, regional end-diastolic wall thickness and systolic wall thickening provide useful information for the assessment of the location, extent and severity of ventricular abnormalities in ischemic heart disease. MRI can also be used to study blood flow and myocardial perfusion. Velocity-encoded cine MRI (VEC-MRI) is often utilized for the quantification of blood flow through the aortic and pulmonary valves and atrio-ventricular valve planes, which has shown to be clinically valuable in the evaluation of patients with complex congenital heart disease.

Typical cardiac MRI examinations generate large data sets of images. To optimally and efficiently extract the relevant clinical information from these data sets dedicated software solutions featuring automated image segmentation and optimal quantification and visualization methods are needed. Quantitative image analysis requires the definition of contours describing the inner and outer boundaries of the ventricles, which is a laborious and tedious task when based on manual contour tracing. Reliable automated or semi-automated image analysis software would be required to overcome these limitations. This paper focuses on the state-of-the-art post-processing techniques for the quantitative assessment of global and regional ventricular function from cardiac MRI.

2.2 Quantification of ventricular dimensions and global function

2.2.1 Accuracy and reproducibility of volumetric measurements from multi-slice short-axis acquisitions

MRI allows imaging of anatomical objects in multiple parallel sections, enabling volumetric measurements using the Simpson's rule. According to this Simpson's rule the volume of an object can be estimated by summation of the cross-sectional area's in each section multiplied by the section thickness. When there is a gap in between slices this must be corrected for and the formula for volume becomes:

$$V = \sum \{Area_i * (Thickness + Gap)\},$$

where V is the volume of the 3D object and $Area_i$ the area of the cross-section in section number i.

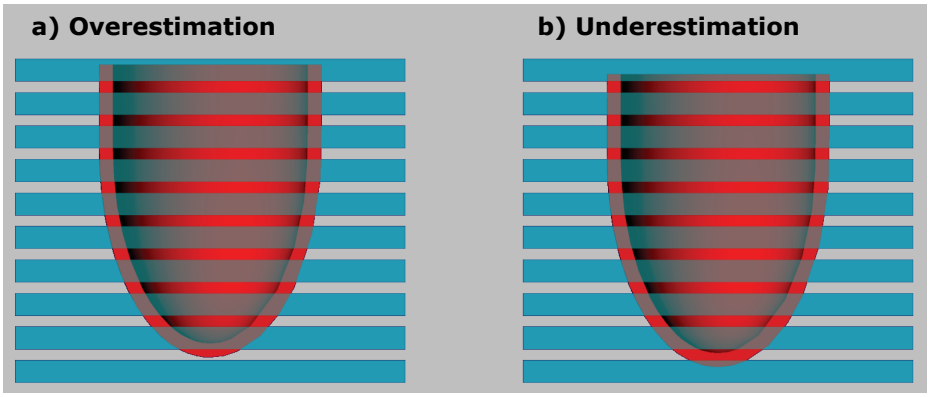

Figure 2-1 Schematic representation of a left ventricular geometry intersected by multiple parallel short-axis sections. Given the same section thickness and intersection gap both over- and underestimation of left ventricular volume may occur dependent on the position of the left ventricle with respect to the imaging slices. In situation a) the most basal slice will be included in the volumetric assessment, while in b), the most basal slice will not be taken into account since it intersect by less than 50% with the left ventricular myocardium.

While MRI is capable of directly acquiring images in any orientation, the short-axis orientation is the most commonly applied image orientation for the assessment of left ventricular chamber size and mass. The short-axis orientation has advantages over other slice orientations since it yields cross-sectional slices almost perpendicular to the myocardium for the largest part of the left ventricle[1]. This results in minimal partial volume effect at the myocardial boundaries and subsequently provides optimal depiction of the myocardial boundaries. However, the curvature of the left ventricle at the apical level leads to significant partial volume averaging. The image voxels in this area simultaneously intersect with blood and myocardium yielding indistinct myocardial boundaries. By minimizing the slice thickness - while keeping sufficient signal to noise - this partial volume effect at the apex can be reduced. Given the relatively small cross-sectional area of the left ventricle in the apical section, the error introduced due to the partial volume effect will be minimal. However, partial volume averaging at the basal level of the heart has a much greater impact since at this level the cross-sectional area of the LV is largest. The base of the LV

exhibits a through-plane motion in the apical direction during systole in the order of 1.3 cm[2,3]. Therefore, the significance of partial volume varies over the cardiac cycle. Additional long-axis views may prove helpful in determining more accurately how a basal short-axis slice intersects with the various anatomical regions.

2.2.2 Impact of slice thickness and slice gap

It is a prerequisite for the accurate assessment of the ventricular volumes that the stack of short-axis slices covers the complete ventricle from base to apex. Typically, a section thickness between 6 and 10 mm is used while the gap between slices varies from no gap (consecutive slices) to 4 mm. Quantification of volumes and mass requires the definition of contours in the images describing the endocardial and epicardial boundaries of the myocardium in several phases of the cardiac cycle. Though an image voxel may contain several tissues – due to the partial volume effect – it is assumed that the traced contours represent the geometry of the ventricle at the center of the imaged section. As shown in Figure 2-1, the partial volume effect may lead to both over- and underestimation in the assessment of ventricular volume.

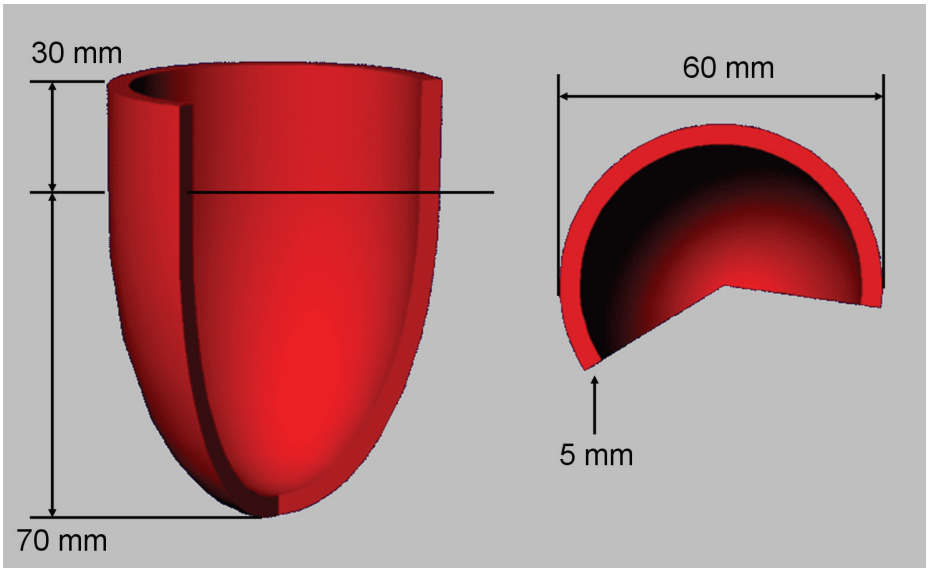

Figure 2-2. Schematic representation of the left ventricular geometry used for the simulation experiments. The phantom consists of a half ellipsoid with a length of 70 mm and an outer diameter at the base of 60 mm; at the base the shape is extended with a cylinder with a diameter of 60 mm and a length of 30 mm. The thickness of the phantom was set to 5 mm. In the experiments the size of the object was varied between the dimensions shown and 80% of this size.

With a simple experiment using synthetically created left ventricular shapes and short-axis cross-sections it can be shown how the partial volume problem may affect measurement accuracy and reproducibility. For this purpose a computer-generated average left ventricular geometry with a fixed size was constructed and short-axis cross-sections were automatically derived, while varying the position of the ventricular geometry along the long-axis direction. The shape used and its dimensions are presented in Figure 2-2. In this experiment it is assumed that the contours in a short-axis slice will only be drawn in case more than 50% of the slice thickness intersects with myocardium. The results of the simulations as depicted in Figure 2-3 demonstrate that the measurement precision (or measurement variability) degrades with increasing distance between the slices. For typical imaging parameters (section thickness 6 mm, gap 4 mm) the measurement variability is between 4 and 5%. The measurement accuracy is not dependent on the slice thickness or slice gap used: a section thickness of 10 mm with no gap results in the same variability as a section thickness of 6 mm with a gap of 4 mm.

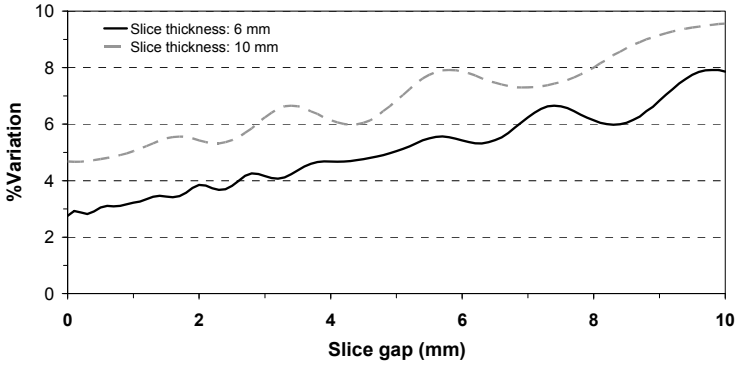

Figure 2-3. Results of volume calculation experiments using synthetically constructed left ventricular geometries. The variability of left ventricular volume estimates increases with increasing slice thickness and slice gap. For a setting of the imaging parameters, such as a thickness of 6 mm and a gap of 4 mm, the measurement variability is ~5%.

The result of this experiment has two important implications. First, variations between successive scans of the same patient may result in volumetric differences of up to 5%, which are inherent to the imaging technique used. Second, since the base of the heart has a significant through-plane motion component, the measurement variability of up to 5% will also be present over the cardiac cycle. Therefore, ejection fraction measurements will also be affected. By reducing the section thickness and the inter-section gap the variability in volumetric measurements can be reduced.

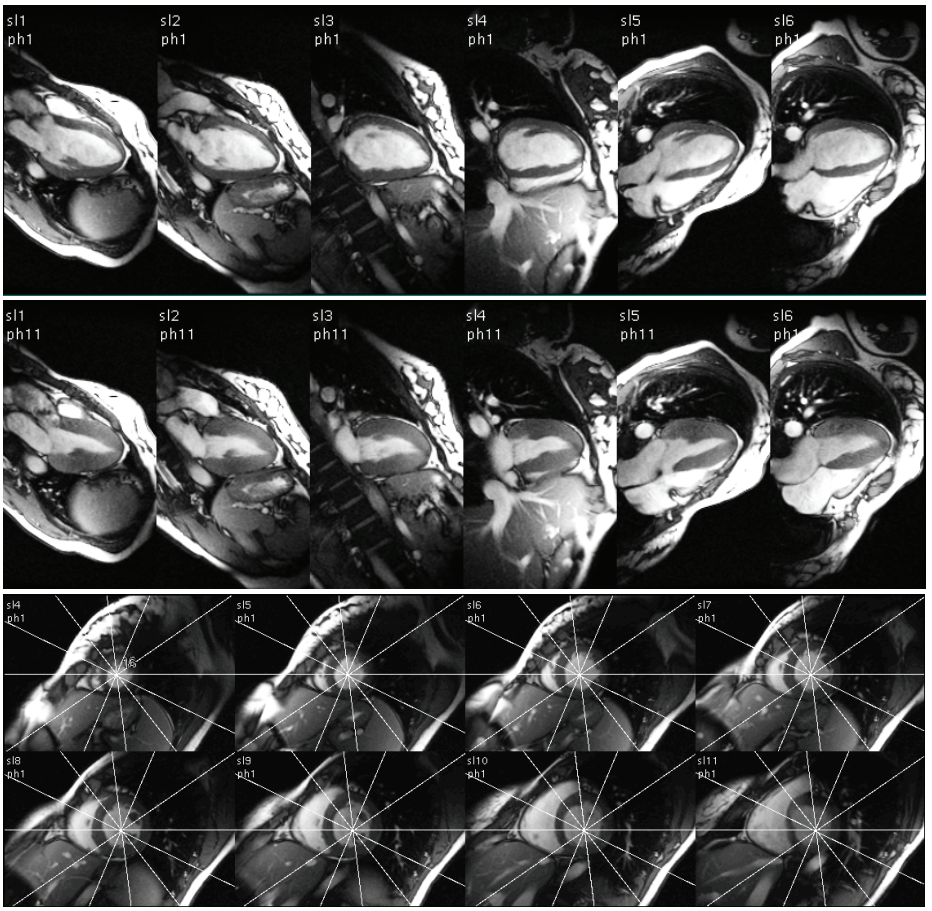

Figure 2-4. ED (top) and ES (middle) MR images acquired in radial long-axis views using SSFP MRI. Note the excellent conspicuity of the LV myocardial wall from base to apex. For reference, the white lines in the short-axis images (bottom) show the orientation of the radial long-axis views. (MR image data courtesy of M. Friedrich)

2.2.3 Global function assessment using radial long-axis views

The accuracy of volumetric measurements from multi-slice short-axis acquisitions is mainly determined by the accurate identification of the most basal slice level and the accurate definition of the endocardial and epicardial contours in this slice level. However due to the relatively large section thickness used, this is often difficult. The origin of the problem is the highly anisotropic nature of a typical short-axis examination in which the resolution in the Z-direction is much worse than the in-plane resolution. In order to overcome this limitation, Bloomer *et al*. investigated the use of multiple radial long-axis views for quantification of left ventricular volumes and mass using an SSFP MRI sequence[3]. With a radial long-axis acquisition

multiple long-axis views are acquired sharing a common axis of rotation (the LV long-axis) at equiangular intervals. This orientation has intrinsic advantages over short axis imaging as it allows clear visualization of the mitral and aortic valve planes. Additionally, long axis views suffer less from partial volume effect near the apex. After definition of the ventricular contours, calculation of LV volume is performed by adding pie-shaped volume elements defined by the location of the axis of rotation, the position of the contour and the angular interval between the image sections. Bloomer *et al*. demonstrated a good agreement between multi-slice short-axis and radial long-axis acquisitions. Importantly, as a result of the improved visualization of the myocardial boundaries and definition of the base, inter-observer agreement was better using the radial long-axis method. Clay at al. presented gender specific normal values for left ventricular volume and function parameters assessed using the radial long-axis approach[5]. Figure 2-4 illustrates examples of MR images acquired using a radial long-axis orientation. It clearly shows that the definition of the base and the contrast between blood and myocardium is excellent. Further research is needed to evaluate whether radial long-axis acquisitions also prove to be valuable for the assessment of regional function.

2.3 MYOCARDIAL MASS

The measurement of heart muscle weight is of clinical importance to properly diagnose and understand a patient's illness and condition, and to estimate the effects of treatment. To detect small changes in mass, it is of paramount importance to utilize an accurate and reproducible measurement technique. Several validation studies have been performed comparing mass estimates as derived from MR with postmortem mass measurements. In a study by Florentine *et al*. a stack of axial slices was used to quantify left ventricular mass using the Simpson rule[6]. In this early study, they found good agreement (r = 0.95, SEE = 13 g). Maddahi *et al*. carried out extensive studies in a dog model comparing several slice orientations and measurement techniques for quantifying left ventricular mass[7]. It was shown that in vivo estimates of left ventricular myocardial mass are most accurate when the images are obtained in the short-axis plane (r=0.98, SEE = 4.9 g).

2.3.1 Left ventricular mass

For the left ventricle it is generally believed and also supported by literature that the short-axis orientation is the most appropriate imaging plane. To obtain optimal accuracy and reproducibility it is important to cover the complete ventricle from apex to base with a sufficient number of slices.

Quantification of mass requires the definition of contours in the images describing the endocardial and epicardial boundaries in the stack of images. The muscle volume is assessed from these contours by applying Simpson's rule. The myocardial mass is derived by multiplying the muscle volume with the specific density of myocardium (1.05 g/cm^3).

Typically, a section thickness between 6 and 10 mm is used with an inter-section gap between 0 and 4 mm. At the apex and basal sections significant partial volume averaging will occur due to the section thickness used and tracing of the myocardial boundaries may not be trivial. Similarly partial volume averaging will cause significant difficulties in interpreting sections with a highly trabeculated myocardial wall and papillary muscles[8]. There is no general consensus on whether to include or exclude papillary muscles and trabeculae in the left ventricular mass[9-13]. While it evident that inclusion of these structures would result in more accurate myocardial mass measurements, for regional wall thickening analysis, it is important to exclude these structures to avoid artifacts in the quantification. Whether to use an end-diastolic or end-systolic time frame for the measurement of the myocardial mass is also a subject of ongoing debate. Most likely, optimal accuracy and reproducibility is obtained by averaging multiple time frames, but this will have practical objections in case contours are derived by manual tracing.

2.3.2 Right ventricular mass

For the right ventricle and also for geometrically abnormal shaped left ventricles multiple sections are required for an accurate volume assessment[14]. MRI experiments with different slice orientations in phantoms and ventricular casts have shown that no significant difference can be observed in accuracy and reproducibility between slice orientations[15]. However, in a clinical situation the choice of slice orientation also depends on the availability of a clear depiction of anatomical features that are needed to define the myocardial boundaries. Volumetric quantification of the right ventricle may be better performed on the basis of axial views[16]. This view shows improved anatomical detail and allows better differentiation between the right ventricular and atrial lumen. Nevertheless, for practical reasons, the right ventricular mass is often measured using a stack of short-axis slices which is also used for measuring the left ventricular dimensions.

2.4 QUANTIFICATION OF VENTRICULAR VOLUMES AND GLOBAL FUNCTION

Assessment of global ventricular function requires volumetric measurement of the ventricular cavities in at least two points in the cardiac cycle, being the end-diastolic (ED) and end-systolic (ES) phases. A vast amount of reports describe the applicability of MRI for accurate and reproducible quantification of left and right ventricular volumes using various MR imaging strategies[4,17]. Sufficient temporal resolution is required to properly capture the end-systolic phase. Generally a temporal resolution, or phase interval, in the order of 40-50 ms is assumed to be sufficient[18].

For geometrically normal left ventricles one could rely on geometrical models to derive the volumes from one or two long-axis imaging sections. In a group of ten patients with LV hypertrophy and 10 healthy subjects, Dulce *et al*. demonstrated a good agreement between biplane volumetric measurements using either the modified Simpson's rule of an ellipsoid model and true 3D volumetric measurements using a multi-slice MRI approach[19]. In another study by Chuang *et al*. 25 patients with dilated cardiomyopathies were evaluated using both a biplane and a 3D multi-slice approach[20]. They reported a poor correlation between the two measurement methods.

For quantitative volume assessment, using multi-slice short-axis acquisitions is the most commonly applied approach. At the present state, a single section with sufficient temporal resolution can be acquired within a single breath hold, on most available MR systems. The total duration of acquiring the 8 to 12 sections required to image the entire ventricular cavity is in the order of 5 minutes[21,22]. All sections should be acquired at the same end-expiration or end-inspiration phase; otherwise reliable 3D-quantification of volumes from the obtained images is not possible.

Quantitative analysis starts with manual or (semi-) automated segmentation of the myocardium and blood pool in the images. Once contours have been defined in the stack of images describing the endocardial and epicardial boundaries of the myocardium, volumetric measurements including stroke volume and ejection fraction can be obtained by applying the Simpson's rule. Normal values for global ventricular function and mass have been reported by several investigators for different populations and pulse-sequences[23-25]. It is important to note that normal values obtained using the newer Steady State Free Precession (SSFP) type sequences differ significantly from values obtained with previous techniques. The improved contrast between blood and myocardium in SSFP is associated with larger ED and ES cavity volumes, smaller wall thickness values and lower LV mass[25-27]. In direct comparisons

of SSFP with conventional fast GRE techniques within the same individuals, differences in LV mass of up to 16.5% were reported (see Figure 2-5). In contrast, LV measurements have been shown to be relatively independent of the MR field strength used[28].

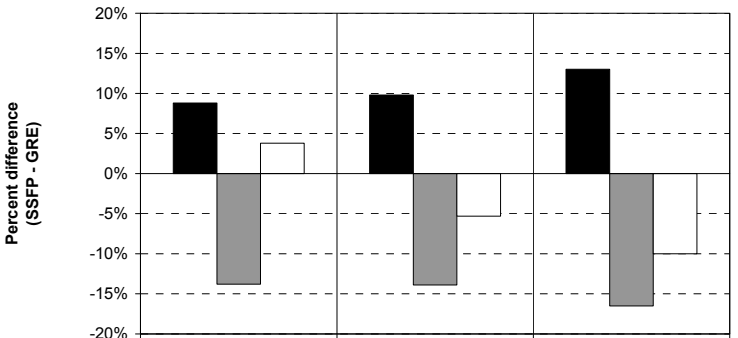

	Philips/TFE	GE/FastGRE	Siemens/FLASH
■ EDV	8.8%	9.80%	13%
▒ LV mass	-13.80%	-13.90%	-16.50%
□ EF	3.80%	-5.30%	-10%

Figure 2-5. Comparison of LV dimensions measured with either a Steady State Free Precession (SSFP) sequence or a segmented GRE technique. Data derived from Alfakih et al[25], Lee et al[26] and Wei et al[27].

At the basal imaging sections, often no clear visual separation between left ventricle and left atrium is present since the imaging section may contain both ventricular and atrial cavity and muscle. It is important to realize that while the imaging sections are fixed in space, the left ventricular annulus exhibits a motion in the apical direction on the order of 1.3 cm in normal hearts[2]. Consequently, myocardium that is readily visible in an end-diastolic time frame may be replaced by left ventricular atrium in the end-systolic time frame. Additional long-axis views may be helpful to more reliably analyze the most basal and apical slice levels of a multi-slice short axis study[3]. Figure 2-6 displays end-diastolic and end-systolic time frames in a long-axis view and three basal short-axis sections obtained during a single MR examination. The white lines, indicating the intersection lines of the imaging planes, provide helpful additional information for interpreting the structures seen in the short-axis images.

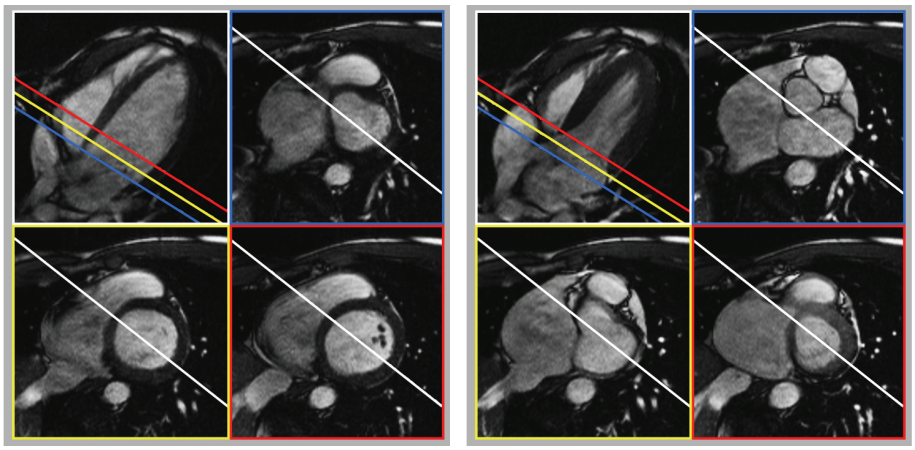

Figure 2-6. Four-chamber long-axis view and three basal level short-axis views acquired within the same examination (left: end-diastole, right: end-systole). The colored lines indicate how the short-axis and long-axis imaging planes intersect with each other. The movement of the base towards the apex in systole can easily be appreciated. The use of displays showing how long-axis and short-axis planes intersect may facilitate the interpretation of basal level short-axis images and may be valuable during tracing of the contours.

2.5 Quantification of regional wall motion and wall thickening using the centerline method from dynamic short-axis images

The excellent depiction of the endocardial and epicardial boundaries of the left ventricular myocardium forms the basis of quantitative analysis of regional myocardial function. Quantitative analysis methods for endocardial wall motion are hampered by the presence of rigid body motion of the heart. A floating centroid, based on the center of gravity of the endocardial or epicardial contours, can be used to isolate the rigid body motion from the actual endocardial deformation. On the other hand, quantification of wall thickness and thickening does not have this disadvantage. It has been demonstrated that wall thickening analysis is more sensitive in the detection of dysfunctional myocardium than wall motion analysis[29,30]. The optimal slice orientation for wall thickness analysis of the left ventricle is the short-axis plane since in this orientation the major part of the myocardial wall is perpendicular to the imaging section[29-33]. Local wall thickness can be derived in these acquisitions from manually or automatically defined endocardial and epicardial boundaries in each short-axis image. Radial wall thickness quantification methods use an approximate center point in the left ventricle to measure the distance between the endocardial and epicardial contours along radial lines starting from this center point. This approach may result in significant

overestimation of wall thickness in case the ventricular cross-section deviates much from a circular shape. The Centerline method has advantages over the radial methods since it can be applied for a wide variety of shapes. In fact, it was originally developed for wall motion analysis in X-ray angiograms and later modified for wall motion and wall thickness analysis of left ventricular short-axis views[35,36].

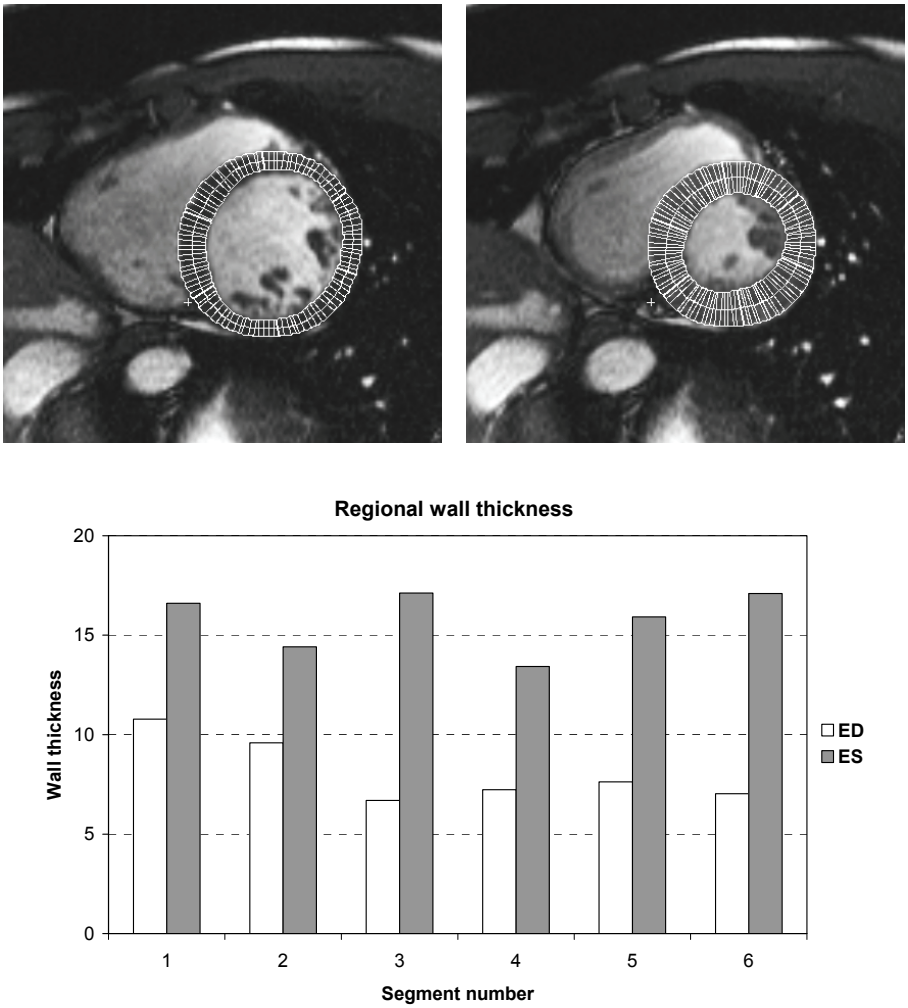

Figure 2-7. Mid-ventricular end-diastolic (top left) and end-systolic (top right) short-axis images of the left ventricle with endocardial and epicardial contours defined. Wall thickness chords are constructed for measurement of wall thickness in six myocardial segments. The segments are defined starting at the posterior junction of the right ventricular wall with the left ventricle. Segments are numbered from 1 through 6 in clockwise order. The graph in the bottom panel presents the wall thickening in each of the six defined myocardial segments.

As depicted in Figure 2-7, the centerline method uses a path in between the endo- and epicardial contours (the "centerline") and perpendicular to that path at evenly spaced intervals, starting at a clearly visible anatomical reference point chords are constructed from endocardium to epicardium. The length of such a chord represents the local wall thickness and the ratio between the end-systolic and end-diastolic chord length equals the local end-systolic wall thickening. A sufficient number of chords should be chosen such as not to miss small anatomical abnormalities. Normal values for end-systolic wall thickening can be used for comparison to determine which myocardial regions are abnormal; subsequently the size, extent and severity of a wall thickening abnormality can be quantified[36]. In case the MRI slice is not exactly perpendicular to the local myocardial orientation, the normal two-dimensional centerline method may lead to a wall thickness overestimation. Buller *et al*. describe a method to correct for this error by estimating the local angle between the imaging plane and the myocardial wall for each centerline chord[37]. They demonstrated the improved accuracy of this method in phantom studies and also showed that the overestimation of wall thickness near the apex of the heart in short-axis studies can be minimized.

To facilitate the interpretation of the large amount of quantitative data of regional ventricular function, optimized visualization methods need to be implemented. When standardized imaging protocols are applied, normal value databases can be established for the various parameters providing more objective assessment of the observed regional function abnormalities. Bull's eye plots, as known from nuclear medicine, can be used as a visual tool to present all the relevant information in just one single graphical display. A further step is to employ three-dimensional reconstruction techniques to generate displays showing regional function data in relation to the anatomy of the patient. Figure 2-8 shows an example of such a display, providing views of the left ventricular anatomy of a patient with an antero-septal infarction.

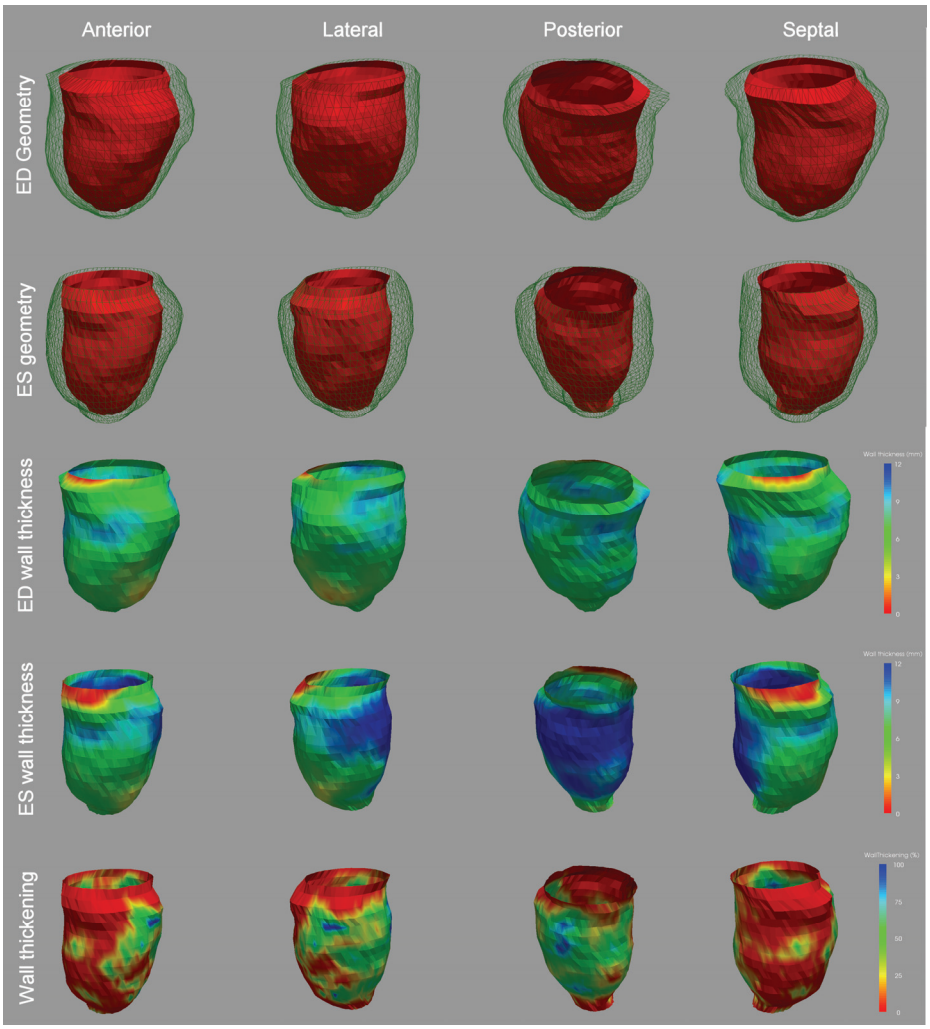

Figure 2-8. Three-dimensional reconstruction of the left ventricle from a multi-slice short-axis study of a patient ten days after acute antero-lateral infarction. The top two rows show the ventricular geometry at the ED and ES phases. The bottom three rows show the ED wall thickness, the ES wall thickness and ES wall thickening using a color-coding.

2.6 Regional function analysis using MRI tagging and velocity-encoded MRI

Wall thickening and wall motion analysis from conventional cine MR imaging suffers from the through-plane motion of the heart. Furthermore, conventional cine MRI only allows quantification of radial myocardial deformation. Three-dimensional myocardial tagging is a powerful MRI

technique that allows quantification of myocardial strain in all three dimensions. With the use of MRI tagging, cine MR images are acquired with a superimposed parallel, rectangular or radial grid of dark saturation lines. These tagging lines are induced by a special pre-pulse sequence immediately following the R-wave of the ECG and can subsequently be followed over the cardiac cycle. Dedicated computer algorithms have been developed to automatically track the intersection points of the tagging lines over the cardiac cycle to be able to quantify intramural myocardial deformations[38]. By applying this technique in multiple slices in both short-axis and long-axis directions, 3D-strain measurements can be performed[39]. Alternatively, these measurements can be derived directly by processing of the Fourier spectrum of the tagged MR data, a technique currently known as HARmonic Phase (HARP) imaging[40,41].

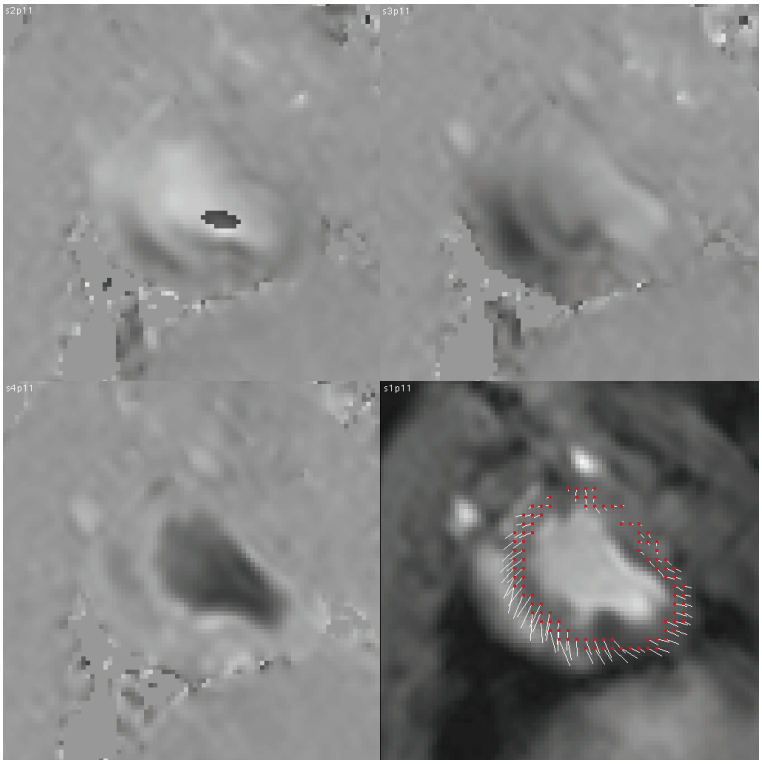

Figure 2-9. Short-axis images obtained by phase-contrast cine MRI at early diastole. The images are obtained from a pig after acute myocardial infarction. The velocity images (x, y, z) depict the myocardial velocities in x, y and z direction using a gray-scale encoding. The in-plane velocity vectors (v) are reconstructed from the x- and y-velocity maps and show both the direction and magnitude of myocardial velocity. The relatively low velocities in the anterio-lateral region illustrate the diastolic function abnormality in this region.

Velocity-encoded cine MRI may be used to quantitatively assess the three-dimensional velocity of the myocardium over the cardiac cycle. With this acquisition technique the myocardial velocities can be measured in three orthogonal directions for each pixel within the imaging plane[42-44]. In contrast to MR tagging methods, this technique can be used in combination with retrospective gating such that data over the complete cardiac cycle is obtained. For quantitative analysis two different approaches can be followed. Motion tracking techniques, which are based on velocity integration, can be applied to obtain two- or three-dimensional trajectories of myocardial sample points[45]. An alternative approach is the direct quantification of myocardial strain-rate by calculating the spatial velocity gradient along different directions[46]. Both approaches are sensitive to imperfections of the images such as insufficient temporal or spatial resolution, blood-related artifacts and beat-to-beat variations. These problems may well be resolved by future improvements in image acquisition techniques.

2.7 Automated contour detection in short-axis multi-slice cine MRI

Despite the fact that the time required for image acquisition has been reduced tremendously over the last few years, a cardiac evaluation based on CMR including quantitative analysis remains time consuming due to the required post processing of the large amount of images. Assuming a ventricle which is imaged in ten imaging sections, twenty endocardial contours need to be defined for the assessment of basic global function parameters such as the ejection fraction and stroke volume. Ten addition epicardial contours are needed for quantification of left ventricular mass. Manual image analysis requires tracing of these myocardial outlines which is a time-consuming procedure that takes between 10 minutes and one hour depending on the software used. It also may introduce undesirable inter- and intraobserver variabilities.

A considerable number of groups, including ours, have contributed to the development of algorithms for the automated extraction of the left ventricular myocardial outlines from short-axis cine MR imaging studies[47-61]. The development of automated contour detection algorithms is a challenging problem because variations in gray value in MRI depend on many factors such as the imaging parameters used, spatial dependency in case surface coils are used and flow dependency. Additionally, the geometry of the cardiac chambers and its contraction pattern may be abnormal in pathological situations, causing automated segmentation methods that rely too much on an expected shape or contraction pattern to fail in such circumstances. Ideally, an automated algorithm should be

insensitive to variations in image characteristics and be applicable to MR images obtained from different MR scanners. In case the algorithm can operate without any user-interaction, the actual computation time is not of major importance. If user interaction is required to control the algorithm, such as providing seed points or initial contours for each of the imaging slices, the actual algorithm should be must faster to increase the time efficiency of the operator.

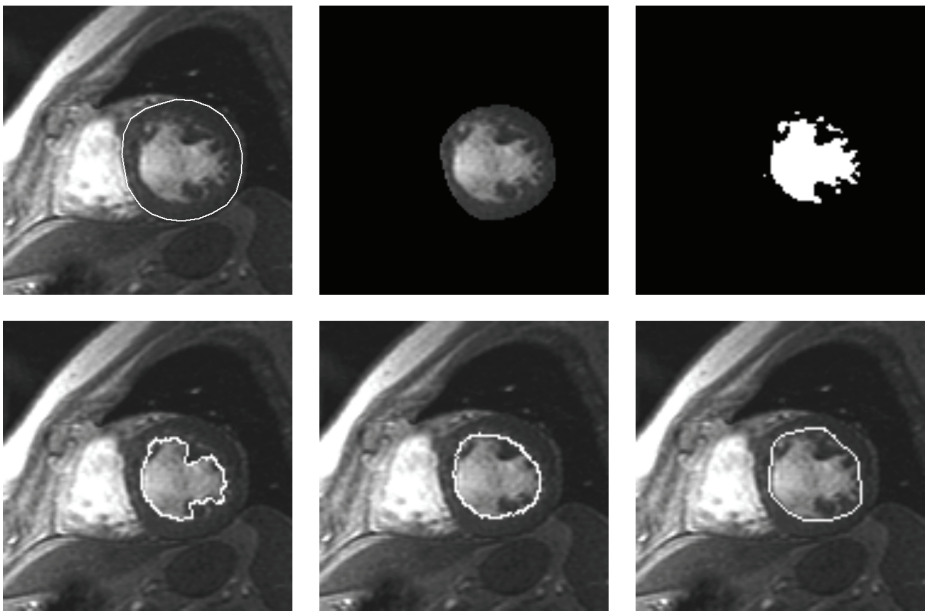

Figure 2-10. Automated detection of the endocardial contour. A) Original image with epicardial contour; B) Search region for the endocardial contour. The region outside the epicardial contour and a small region at the inside of the epicardial contour is masked out from the original image; C) Result after determination of the optimal threshold; D) Contour around the thresholded region serves as a starting contour for the subsequent edge-based contour detection; E) When papillary muscles needs to be excluded from the myocardium, a smooth convex hull contour around the initial contour is determined; F) Final result after minimum cost contour detection.

In the next section a short description is given of the underlying methods and validation results from the algorithms developed at our laboratory which have been integrated in a software package, MASS[51]. Our contour detection method follows a model-based approach and is directed to the definition of the endocardial and epicardial contours in all the phases and slices of an imaging study. The amount of user-interaction required to obtain reliable contours is limited, and is minimal in case the images are of good quality. The algorithm accommodates for anatomical and MRI related

variations in image appearance by providing a certain learning behavior. Manually traced or edited contours are assumed to be correct and the contour detection algorithm was designed to generate a consistent set of contours for the total image dataset using the manually defined contours as models. The contour detection starts by searching for circular objects in the imaging slices to find the approximate long axis of the left ventricle, which result in an approximate left ventricular center point in each image. Using this center point, epicardial contours are found in the first phase and subsequently in the remaining phases using a frame-to-frame contour detection procedure. This frame-to-frame epicardial contour detection procedure is based on matching of line profiles that are positioned perpendicularly to the model contour (derived from the first phase) and then automatically positioned at the corresponding tissue transitions in other phases within the same slice level. By this approach the algorithm is able to deal with the fact that the epicardial boundary of the myocardium is adjacent to regions having different gray value characteristics. A first estimate of the endocardial contour is found using an optimal thresholding technique within the region described by the epicardial contour. The final endocardial contour is found by using a model-based edge-detection technique, known as the Minimum Cost Algorithm[62]. Figure 2-10 illustrates the algorithmic steps that are carried out to detect an endocardial contour given an image with an available epicardial contour.

2.7.1 Automated contour detection optimization for different MR pulse sequences

A major challenge when designing and implementing a reliable automated contour detection algorithm is to deal with the large variations in image characteristics due to differences in MR pulse sequences used, the usage of different receiver coils and differences between MR scanners from different vendors. Consequently, for optimal performance, an automated segmentation method needs to be optimized for a specific type of acquisition procedure. We have recently developed a contour detection optimization procedure, which enables tuning the different parameters that control the automated contour detection[63]. Figure 2-11 illustrates the mechanism of the contour detection tuning method. Based on a set of short-axis exams with expert drawn reference contours available, automated contour detection is performed using different settings of the contour detection procedure. Contour detection settings that are varied are the convolution kernels that are used for edge detection in the images, parameters that control the smoothness of the detected contours and many others. The automatically detected contours generated using a specific

parameter setting are compared to the reference contours by computing the degree of similarity between both contour sets. A Genetic Algorithm is used to generate new sets of parameter settings based on the results of the previously evaluated sets. By iterating this procedure numerous times, an optimal set of parameters can be found for a specific set of images. The degree of similarity, which is used to evaluate the quality of the detected contours, is defined as the percentage of contour points that lie within a 2 mm distance of the corresponding reference contour. It was shown that for SSFP type acquisitions, the degree of similarity for manually traced endocardial contours obtained by repeated analysis of the same observer was 77%. Therefore, since the reference contours are generated manually, the similarity between automatically detected contours and the reference contours has a theoretical upper bound of 77%. The described optimization approach was evaluated on a set of 30 SSFP examinations from the three main MR scanner vendors to assess the improvement in the performance of automated contour detection. In all 30 studies endocardial contours were carefully traced in the end-diastolic and end-systolic phases which were used as reference. Automated contour detection was performed in all studies with and without optimized settings. When using the unoptimized settings the average degree of similarity was 49.5%, which increased to 63.3 percent when using the optimized settings.

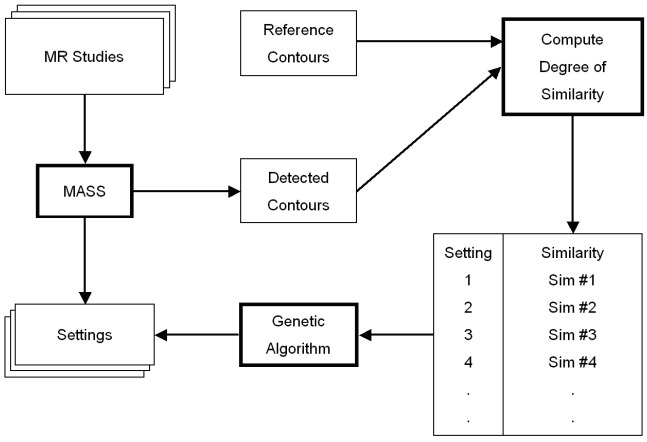

Figure 2-11. Diagram of the automated optimization procedure to find the optimal contour detection settings for a specific pulse sequence. In an iterative procedure, MASS performs automated contour detection in a set of MR studies using a number of different parameter settings. The detected contours are compared to manually defined reference contours and the average degree of similarity is computed for each parameter setting. A Genetic Algorithm is used to generate new parameter settings based on the results of the parameter settings from the previous iteration.

2.7.2 New model-based automated segmentation methods

Reliable fully automated contour detection, not requiring any user interaction, would clearly be an important step to further improve the clinical utility of CMR. Despite a lot of research in this area, two major problems limit the success rate of many of the previously described contour detection strategies for cardiovascular structures. First, due to the presence of noise and image acquisition artifacts, image information can be ill defined, unreliable or missing. In these cases a human observer is still capable of tracing the myocardial contours in the image data based on experience and prior knowledge, while many automated techniques fail. Second, a contour as drawn by an expert human observer may not always correspond to the location of the strongest local image evidence. In particular, in short-axis images the papillary muscles and trabeculae pose a problem. For example, many experts prefer to draw the left ventricular endocardial border as a convex hull around the blood pool, at a location somewhat 'outside' of the strongest edge[64,65]. A second example is the epicardial boundary, which may be embedded in fatty tissue, as a result of which the edge is strongest at the fat-air transitions. However, often the contour should be drawn on the inside of this fatty layer, an intensity transition that is marked by only a faint edge. Therefore, a decision about the exact location of the contour cannot always be made based on the strongest image evidence, but should be learned from the examples and preferences provided by expert observers.

To overcome these problems, prior knowledge about the image appearance, spatial organ embedding, characteristic organ shape and its anatomical and pathological shape variations should form an integral part of a contour detection approach. Moreover, it should be adaptive to accommodate for the preferences of an observer and to be easily adjustable to image characteristics of various pulse sequences and MR systems. Recently, Cootes *et al*. introduced the concept of Active Appearance Models (AAM's), which are trainable mathematical models that can learn the shape and appearance of an imaged object from a set of example images[66]. This method was originally developed for facial recognition and later optimized for the detection of the left ventricle in CMR[67]. An AAM consists of two components: a statistical model of the *shape* of an object, which is combined with a statistical model of the *image appearance* of the object in a set of example images. The combined model is trained to learn the shape and image structure of an organ from a representative set of example images from different subjects. The AAM can be automatically matched to a new study image by minimizing an error function expressing the difference between the model and the underlying

image evidence. During this matching process, the model is constrained to only resemble statistically plausible shapes and appearances. Consequently, AAM's are able to capture the association between observer preference and the underlying image evidence, making the AAM's highly suitable to model the expert observer's analysis behavior. Moreover, AAM's can model multiple objects (in our case the left- and right cardiac ventricles) in their spatial embedding. In a study by Mitchell *et al*. this AAM technique showed excellent agreement with manually defined contours, both for the left- and right ventricle simultaneously[68]. Figure 2-12 shows examples of automatically detected contours for the left and right ventricle obtained using this approach. Van der Geest *et al*. investigated the value of incorporating image information of complete time-series in an AAM based contour detection method[69]. The advantage of this approach lies in the fact that information from a complete time-series is used during training and detection, which results in consistent time-continuous segmentation results, even in the presence of image frames with poor image quality.

Another interesting recent development is the use of three-dimensional statistical shape models for ventricular image segmentation. For example van Assen et al have successfully applied 3D Active Shape Models (ASM) for myocardial boundary detection in multi-slice short axis MR studies[70].

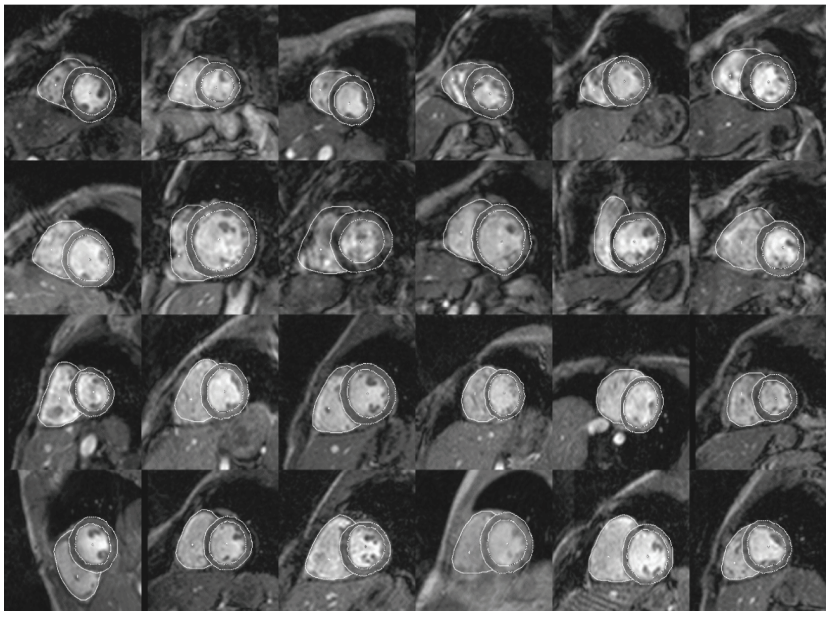

Figure 2-12. Examples of detection results of left and right ventricular contours using the Active Appearance Model contour detection method.

2.8 MRI FLOW QUANTIFICATION

Velocity-encoded cine MRI (VEC-MRI) also plays an important role in the evaluation of global ventricular function. The accuracy of this imaging technique has been demonstrated in *in-vitro* experiments using flow phantoms and comparison against other imaging techniques such as Doppler echocardiography and invasive oximetry[71,72]. Since flow measurements are obtained at high temporal resolution over the complete cardiac cycle, VEC-MRI is especially useful in the evaluation of left and right ventricular diastolic function parameters by measuring flow over the atrio-ventricular valves. Application of this technique to the proximal portion of the ascending aorta or pulmonary artery allows the assessment of left and right ventricular systolic function. After the cross section of a vessel is identified in the image by manual or automated contour detection, the instantaneous flow rate within the vessel cross section is obtained by multiplying the average velocity within the contour by its area. Ventricular stroke volume measurements are derived by integrating the flow over a complete cardiac cycle[73]. The presence of aortic or pulmonary regurgitation can be easily identified and quantified from the derived flow curve. VEC-MRI has an established role in the evaluation of patients with congenital heart disease[74-77]. Figure 2-13 illustrates how MR flow measurement can be used for quantification of shunt size in a patient with a ventricular septal defect.

2.8.1 Automated quantification of aortic flow

Application of VEC-MRI to the proximal portion of the ascending aorta allows the assessment of left ventricular systolic function by evaluating the flow over a complete cardiac cycle. Such a study requires a VEC-MRI acquisition in the transversal plane crossing the ascending aorta. The left ventricular stroke volume can be measured by integrating the flow over a complete cardiac cycle. For an accurate assessment of volume flow, contours describing the lumen of the vessels have to be obtained in the images. The in-plane motion of the greater vessels and changes in shape of the vessel cross section over the cardiac cycle would require the user to trace the luminal border of the vessel in each individual phase of the MR examination. To overcome these practical limitations, an automated analysis method was developed in our department to automatically detect the required contours in each of the cardiac phases[78]. This contour detection algorithm was integrated in the FLOW software package.

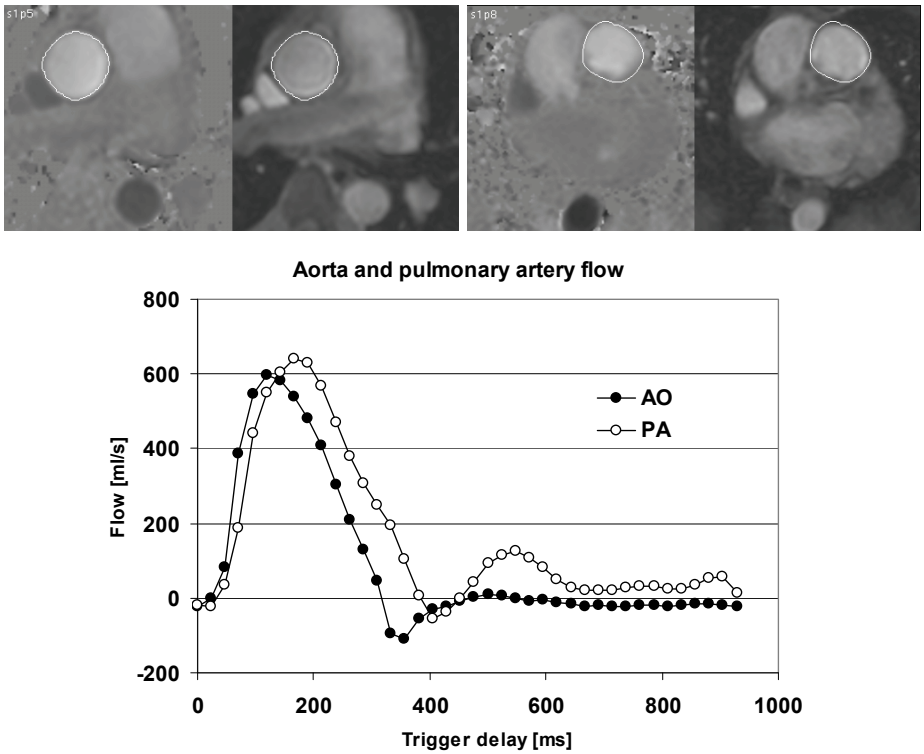

Figure 2**-**13**.** Flow velocity maps of the ascending aorta (top left) and pulmonary artery (top right) with contours defined of a patient with a ventricular septal defect. From the derived flow curves (bottom) of the respective arteries the shunt size can be accurately quantified. In this patient the aortic flow was quantified as 87 ml/heart beat (5.6 L/min) and the pulmonary flow 149 ml/heart beat (9.4 L/min).

The only user-interaction required, is the manual definition of an approximate center in one of the available images. In this first image an initial model contour is detected using gray value and edge information. The position of the same vessel at another time frame can be estimated by shifting the model contour in a limited region around the initial location and examining the edge values measured in the modulus image along the contour points. An algorithm was developed which finds the most likely contour position for each time frame, with the restriction that a contour is only allowed to displace 2 pixels (1.6 mm) from phase to phase, thereby imposing a temporal continuity of the motion. After having found the correct contour location, a final optimized contour was detected by allowing small deformations of the model contour such that it would follow the edges in the modulus image. For this purpose a two-dimensional graph searching technique was used. The resulting contour was dilated by one pixel to be sure to encompass the complete region with flowing blood. The

total contour detection process takes less than ten seconds for a study with 30 cardiac phases.

Validation was performed on flow velocity maps from a study population of 12 healthy volunteers. Two independent observers performed manual and automated image analyses. The first observer repeated the automated and manual analyses after a two-week interval to avoid learning effects. The time required for manual analysis was 5-10 minutes. During automated analysis the user had to identify the approximate location of the center of the aorta in one of the available images. The total analysis time for automated analysis was less than 10 seconds. Stroke volume measurements were obtained by integrating the flow over the complete cardiac cycle. The mean left ventricular stroke volume obtained by VEC-MRI in the group of 12 volunteers was 86.4 ml (SD: 13.6 ml). No statistically significant differences were found between the results of manual and automated analyses. The mean difference between automated and manually assessed stroke volume was 0.78 ml (SD: 1.99 ml). The intra-observer variability was 0.65 ml for manual analysis and 0.58 ml for automated analysis; the intra-observer variability was 0.99 ml for manual analysis and 0.90 ml for automated analysis. From this study, it can be concluded that the automated contour detection algorithm performs equally well as the manual method in the determination of left ventricular stroke volume derived from VEC-MRI studies of the ascending aorta.

2.9 Image processing of perfusion imaging studies

First-pass contrast-enhanced MR perfusion imaging is used to detect abnormalities in myocardial blood flow, related to coronary artery disease. Typically, three to five short axis slices of the heart are acquired over 5 to 10 seconds prior to the injection of the intravenous contrast bolus, and about 60 seconds after the injection of contrast. A combination of stress and rest acquisitions can be performed to improve the differentiation of normal from abnormally perfused myocardial territories[79].

Various approaches have been described to obtain quantitative indices of myocardial perfusion from first-pass MR perfusion studies[80-82]. Jerosch-Herold *et al*. have performed extensive studies to demonstrate the feasibility of absolute perfusion quantification in ml/gram tissue/minute and have validated these methods in animal experimental studies[80]. However, more commonly, semi-quantitative analysis methods are being used. An example of a semi-quantitative approach is to use the maximal upslope of the myocardial time-intensity curve as index of myocardial perfusion. Although less-advanced, the diagnostic accuracy of the technique has been

validated against competing non-invasive and invasive modalities in single center and multicenter studies[83-85].

To derive quantitative indices related to the presence or absence of myocardial perfusion deficits, time-intensity curves need to be evaluated for regions in the myocardium. Due to the significant patient motion over the acquisition duration, time-intensity curves which are derived from a static region in the image are severely distorted. Automated image co-registration techniques have been developed to correct for this motion[86-89]. Once the images are registered, endocardial and epicardial contours can be traced in one image frame and copied to the other frames. Subsequently, time-intensity curves can be easily generated for multiple regions in the myocardium. Although these curves can be determined at a pixel level, the noise level in the images is often not sufficient to derive reliable perfusion indices at this level of detail. More typically 4 to 8 segments are defined for each imaging section, which can be further sub-divided into an endocardial and an epicardial layer[85].

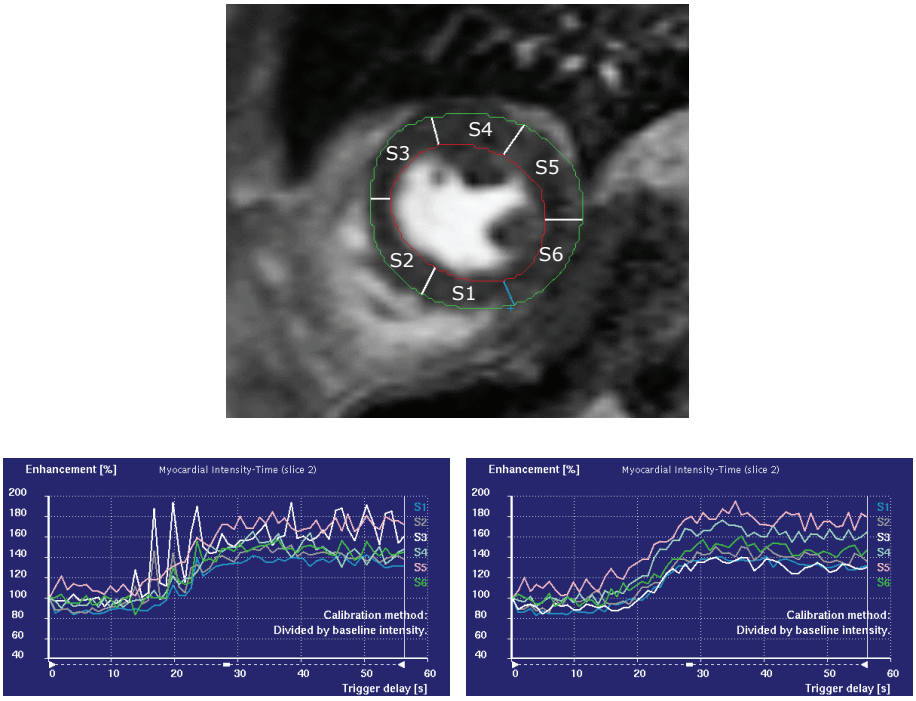

Figure 2-14. Signal-intensity versus time curves for 6 segments of the left ventricular myocardium at a mid ventricular slice level. Without motion correction (lower left) the curves are not suitable for quantitative analysis. After motion correction (lower right), perfusion indices such as maximum upslope can be derived reliably.

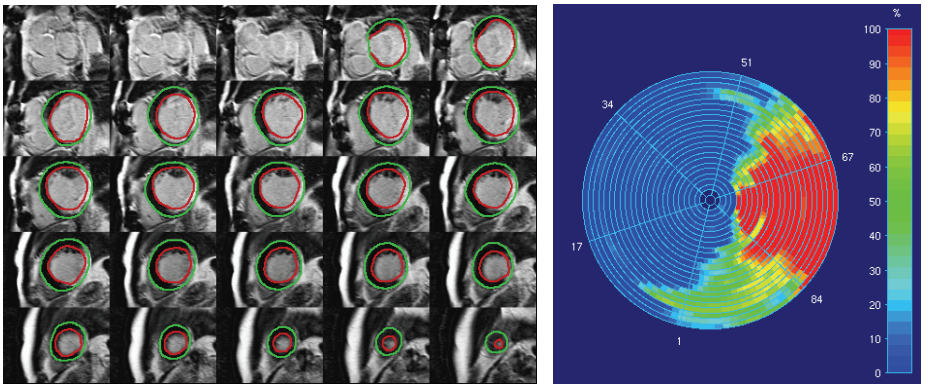

Figure 2-15. Example multi-slice short-axis LGE acquisition (left). After defining an appropriate intensity threshold, the regional transmurality of scar can be computed and visualized using a bull's-eye plot (right). This patient has a large infarction with complete transmural enhancement in the lateral region and sub-endocardial enhancement in the posterior region.

2.10 Late Gadolinium enhanced MRI

Late gadolinium enhanced (LGE) MRI has become part of a standard MRI examination as it is extremely valuable for the assessment of viable and non-viable myocardium in infarcted and poor contractile areas[90,91]. The excellent resolution of MRI enables the depiction of both transmural and non-transmural regions of infarction. It was shown that the transmural extent of enhancement is inversely related to the likelihood of recovery of function after revascularization. Therefore, large non-transmural infarcts may have a better prognosis than relatively small transmural infarcts. Quantification of the size and distribution of the infarction involves defining a signal intensity threshold that separates normal myocardium from enhanced tissue. Various approaches have been suggested for determining the optimal intensity threshold. In the pioneering work of Kim et al. hyper-enhanced regions were defined as those regions having an intensity value >2D above the mean of the remote normal myocardium[90.] Other authors have suggested slight modifications to this approach by proposing adding 2-5 times the standard deviation[93,94]. These observations demonstrate the sensitivity of the SD-method to differences in image acquisition protocol. Schuijf *et al*. and Amado *et al*. proposes to use a Full Width Half Maximum (FWHM) criterion to objectively obtain a threshold value[95,96]. Amado *et al*. demonstrated in an animal experimental study that myocardial infarct size measurements using a FWHM criterion agreed very well with pathology[96]. The inherent properties of the Full-Width-Half-Max method makes it much less sensitive to variations in image acquisition parameters. Based on this criterion Hsu et al. developed a fully automated technique to obtain

accurate assessment of the size of myocardial infarction and validated this approach in an animal experimental setting[97]. Using the defined threshold, the enhanced regions within the myocardium are objectively defined and the regional degree of transmurality can be defined as illustrated in Figure 2-15.

2.11 Integrated image analysis

The increasing routine clinical use of CMR and the overwhelming size of the typical CMR image data sets pose a significant challenge for time-efficient image quantification and interpretation. Multiple software packages with automated image segmentation and quantification methods have been introduced in the last decade to support the work of the clinician. However, these solutions primarily focus on particular elements within a CMR exam, such as the assessment of global function or myocardial perfusion. An integration of the available techniques for CMR image analysis into an integrated solution for the analysis of all the data acquired in a comprehensive CMR exam would be a major step forward. The work by Hennemuth *et al*. demonstrates the feasibility of such integrated image analysis solutions[98].

An example of an integrated analysis approach is provided in Figure 2-16. It illustrates how quantitative information obtained form two different MR acquisitions can be combined. In this example LGE MRI is combined with cine MRI information to relate infarct transmurality to the regions with poor contractility. This enables classification of regions of poor contractility into viable and non-viable regions.

2.12 Conclusion

Cardiovascular MRI is a valuable technique for non-invasive quantitative assessment of global and regional ventricular function. Computerized image analysis techniques can help reducing the time required for quantification and interpretation of the many images. In this chapter, analytical methods for left ventricular function and vascular flow measurements based on automated contour detection approaches have been described. Validation studies of these methods have confirmed their accuracy, precision, robustness and usefulness for clinical research studies. Fully automated contour detection methods that operate reliably in a routine clinical environment are needed and may become available in the near future.

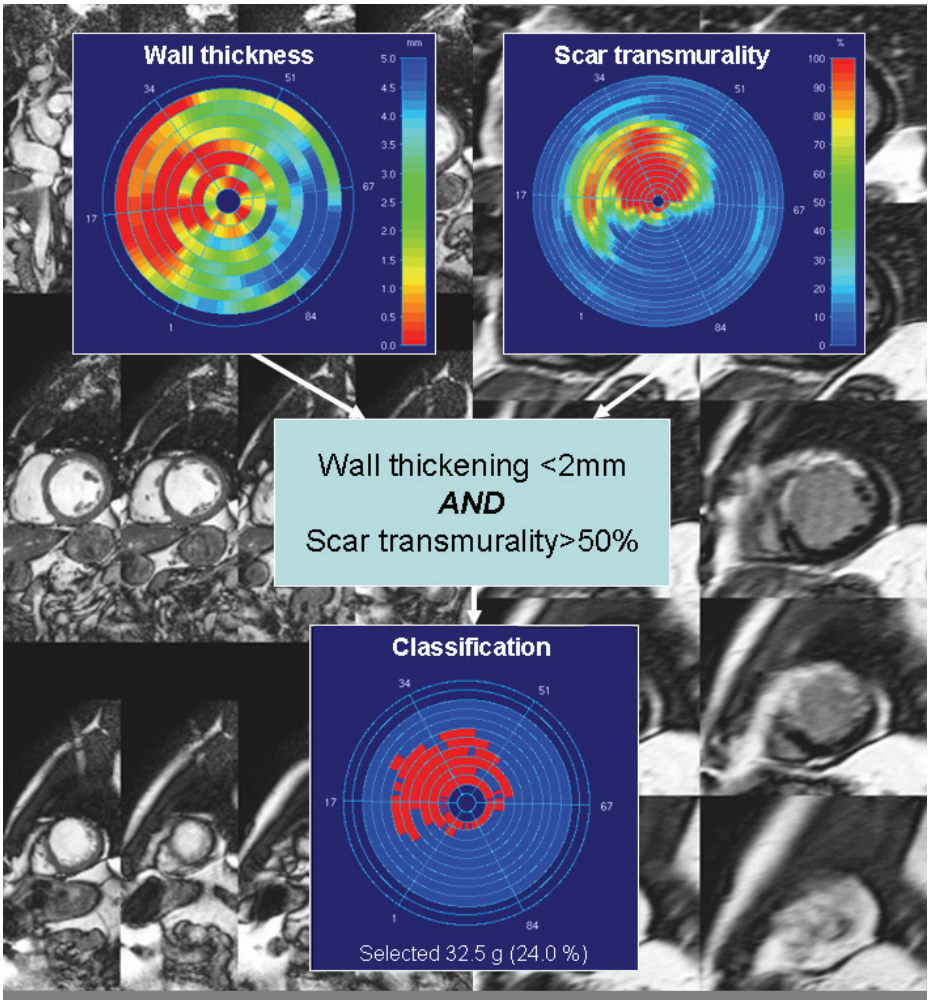

Figure 2-16. Data fusion between wall thickening information derived from cine MR and a scar transmurality derived from LGE MRI visualized using a bulls-eye displays. The red area in the bottom bull's-eye represents the non-viable myocardium where the wall thickening is less than 2 mm while scar transmurality is >50%.

2.13 References

1. Cottin Y, Touzery C, Guy F, Lalande A, Ressencourt O, Roy S, Walker PM, Louis P, Brunotte F, Wolf JE. MR imaging of the heart in patients after myocardial infarction: effect of increasing intersection gap on measurements of left ventricular volume, ejection fraction and wall thickness. Radiology 1999; 213:513-520.
2. Rogers WJ, EPS, Weiss JL, Buchalter MB, Rademakers FE, Weisfeldt ML, Zerhouni EA. Quantification and correction for left ventricular systolic long-axis shortening by magnetic resonance tissue tagging and slice isolation. Circulation 1991; 84:721-731.

3. Marcus JT, Götte MJW, de Waal LK, Stam MR, van der Geest RJ, Heethaar RM, van Rossum AC. The influence of through-plane motion on left ventricular volumes measured by magnetic resonance imaging: implications for image acquisition and analysis. J Cardiovasc Magnetic Resonance 1998; 1:1-6.
4. Bloomer TN, Plein S, Radjenovic A, Higgins DM, Jones TR, Ridgeway JP, Sivananthan MU. Cine MRI using steady state free precession in the radial long axis orientation is a fast accurate method for obtaining volumetric data of the left ventricle. J Magn Res Imag 2002; 14:685-692.
5. Clay S, Alfakih K, Radjenovic A, Jones T, Ridgway JP, Sinvananthan MU. Normal range of human left ventricular volumes and mass using steady state free precession MRI in the radial long axis orientation. MAGMA 2006;19:41-45.
6. Florentine MS, Grosskreutz CJ, Chang W, Hartnett JA, Dunn VD, Ehrhardt JC, Fleagle SR, Collins SM, Marcus ML, Skorton DJ. Measurement of left ventricular mass in vivo using gated nuclear magnetic resonance imaging. J Am Coll Cardiol 1986; 8:107-112.
7. Maddahi J, Crues J, Berman DS, Mericle J, Becerra A, Garcia EV, Henderson R. Noninvasive quantitation of left ventricular mass by gated proton magnetic resonance imaging. J Am Coll Cardiol 1987; 10:682-692.
8. Matheijssen NAA, Baur LHB, Reiber JHC, van der Velde EA, van Dijkman PRM, van der Geest RJ, de Roos A. Assessment of left ventricular volume and mass by cine-magnetic resonance imaging in patients with anterior myocardial infarction intra-observer and inter-observer variability on contour detection. Int J Cardiac Imag 1996; 12:11-19.
9. Sievers B, Kirchberg S, Bakan A, Franken U, Trappe HJ. Impact of papillary muscles in ventricular volume and ejection fraction assessment by cardiovascular magnetic resonance. J Cardiovasc Magn Reson. 2004;6:9-16.
10. Papavassiliu T, Kühl HP, Schröder M, Süselbeck T, Bondarenko O, Böhm CK, Beek A, Hofman MM, van Rossum AC. Effect of endocardial trabeculae on left ventricular measurements and measurement reproducibility at cardiovascular MR imaging. Radiology. 2005;l;236:57-64.
11. Vogel-Claussen J, Finn JP, Gomes AS, Hundley GW, Jerosch-Herold M, Pearson G, Sinha S, Lima JA, Bluemke DA. Left ventricular papillary muscle mass: relationship to left ventricular mass and volumes by magnetic resonance imaging. J Comput Assist Tomogr 2006;30:426-432.
12. Kirschbaum S, Aben JP, Baks T, Moelker A, Gruszczynska K, Krestin GP, van der Giessen WJ, Duncker DJ, de Feyter PJ, van Geuns RJM. Accurate Automatic Papillary Muscle Identification for Quantitative Left Ventricular Mass Measurements in Cardiac Magnetic Resonance Imaging Acad Radiol 2008;15:1227-1233.
13. Janik M, Cham MD, Ross MI, Wang Y, Codella N, Min JK, Prince MR, Manoushagian S, Okin PM, Devereux RB, Weinsaft JW. Effects of papillary muscles and trabeculae on left ventricular quantification: increased impact of methodological variability in patients with left ventricular hypertrophy. J Hypertens. 2008;26:1677-1685.
14. Niwa K, Uchishiba M, Aotsuka H, Tobita K, Matsuo K, Fujiwara T, Tateno S, Hamada H. Measurement of ventricular volumes by cine magnetic resonance imaging in complex congenital heart disease with morphologically abnormal ventricles. Am Heart J 1996; 131:567-575.
15. Jauhiainen T, Järvinen VM, Hekali PE, Poutanen VP, Penttilä A, Kupari M. MR gradient echo volumetric analysis of the human cardiac casts: Focus on the right ventricle. J Comp Assist Tomogr 1998; 22:899-903.
16. Alfakih K, Thiele H, Plein S, Bainbridge GJ, Ridgeway JP, Sivananthan MU. Comparison of right ventricular volume measurement between segmented k-space gradient-echo and steady-state free precession magnetic resonance imaging. J Magn Res Imag 2002; 16:253-258.

17. Semelka RC, Tomei E, Wagner S, Mayo J, Kondo C, Suzuki J, Caputo GR, Higgins CB. Normal left ventricular dimensions and function: Interstudy reproducibility of measurements with cine MR imaging. Radiology 1990; 174:763-768.
18. Miller S, Simonetti OP, Carr J, Kramer U, Finn JP. MR Imaging of the heart with cine true fast imaging with steady-state precession: influence of spatial and temporal resolutions on left ventricular functional parameters. Radiology. 2002;223:263-269.
19. Dulce MC, Mostbeck GH, Friese KK, Caputo GR, Higgins CB. Quantification of left ventricular volumes and function with cine MR imaging: comparison of geometrical models with three-dimensional data. Radiology 1993; 188:371-376.
20. Chuang ML, Hibberd MG, Salton CJ, Beaudin RA, Riley MF, Parker RA, Douglas PS, Manning WK. Importance of imaging method over imaging modality in noninvasive determination of left ventricular volumes and ejection fraction: assessment by two- and three-dimensional echocardiography and magnetic resonance imaging. J Am Coll Cardiol 2000; 35:477-484.
21. Sakuma H, Fujia N, Foo TKF, Caputo GR, Nelson SJ, Hartiala J, Shimakawa A, Higgins CB. Evaluation of left ventricular volume and mass with breath-hold cine MR imaging. Radiology 1993; 188:377-380.
22. Lamb HJ, Singleton RR, van der Geest RJ, Pohost GM, de Roos A. MR imaging of regional cardiac function: Low-pass filtering of wall thickness curves. Magnetic Resonance in Medicine 1995; 34:498-502.
23. Lorenz CH, Walker ES, Morgan VL, Graham TP, Klein SS. Normal human right and left ventricular mass, systolic function and gender differences by cine magnetic resonance imaging. J Cardiovasc Magn Reson 1999; 1:7-21.
24. Rominger MB, Bachmann GF, Pabst W, Rau WS. Right ventricular volumes and ejection fraction with fast cine MR imaging in breath-hold technique: Applicability, normal values from 52 volunteers, and evaluation of 325 adult cardiac patients. J Magn Reson Imag 1999; 10:908-918.
25. Alfakih K, Plein S, Thiele H, Jones T, Ridgway JP, Sivananthan MU. Normal human left and right ventricular dimensions for MRI as assessed by turbo gradient echo and Steady-State Free Precession imaging sequences. J Magn Res Imag 2003; 17:323-329.
26. Lee VS, Resnick D, Bundy JM, Simonetti OP, Lee P, Weinreb JC. Cardiac function: MR evaluation in one breath hold with real-time True Fisp imaging with steady-state precession. Radiology 2002; 222:835-842.
27. Wei LI, Stern JS, Mai VM, Pierchala LN, Edelman RR, Prasad PV. MR assessment of left ventricular function: Quantitative comparison of fast imaging employing steady-state acquisition (FIESTA) with fast gradient echo cine technique. J Magn Res Imag 2002; 16:559-564.
28. Maroules CD, McColl R, Khera A, Peshock RM. Interstudy reproducibility of SSFP cine magnetic resonance: impact of magnetic field strength and parallel imaging. J Magn Reson Imaging. 2008 May;27:1139-1145.
29. Azhari H, Sideman S, Weiss JL, Shapiro EP, Weisfeldt ML, Graves WL, Rogers W, Beyar R. Three-dimensional mapping of acute ischemic regions using MRI: wall thickening versus motion analysis. Am J Physiol 1990; 259 (Heart Circ. Physiol. 28):H1492-H1503.
30. van Rugge FP, van der Wall EE, Spanjersberg SJ, de Roos A, Matheijssen NAA, Zwinderman AH, van Dijkman PRM, Reiber JHC, Bruschke AVG. Magnetic resonance imaging during dobutamine stress for detection of coronary artery disease; quantitative wall motion analysis using a modification of the centerline method. Circulation 1994; 90:127-138.
31. Haag UJ, Maier SE, Jakob M, Liu K, Meier D, Jenni R, Boesiger P, Anliker M, Krayenbuehl HP. Left ventricular wall thickness measurements by magnetic resonance: a validation study. Int J Cardiac Imag 1991; 7:31-41.

32. Baer FM, Smolarz K, PT, Voth E, HS, Sechtem U. Regional 99mTc-methoxyisobutyl-isonitrile-uptake at rest in patients with myocardial infarcts: comparison with morphological and functional parameters obtained from gradient-echo magnetic resonance imaging. Eur Heart J 1994; 15:97-107.
33. Holman ER, Vliegen HW, van der Geest RJ, Reiber JHC, van Dijkman PRM, van der Laarse A, de Roos A, van der Wall EE. Quantitative analysis of regional left ventricular function after myocardial infarction in the pig assessed with cine magnetic resonance imaging. Magn Reson Med 1995; 34:161-169.
34. Sheehan FH, Bolson EL, Dodge HT, Mathey DG, Schofer J, Woo HK. Advantages and applications of the centerline method for characterizing regional ventricular function. Circulation 1986; 74:293-305.
35. von Land CD, Rao SR, Reiber JHC. Development of an improved centerline wall motion model. Comput Cardiol 1990;687-690.
36. Holman ER, Buller VGM, de Roos A, van der Geest RJ, Baur LHB, van der Laarse A, Bruschke AVG, Reiber JHC, van der Wall EE. Detection and quantification of dysfunctional myocardium by magnetic resonance imaging: A new three-dimensional method for quantitative wall-thickening analysis. Circulation 1997; 95:924-931.
37. Buller VGM, van der Geest RJ, Kool MD, van der Wall EE, de Roos A, Reiber JHC. Assessment of regional left ventricular wall parameters from short-axis MR imaging using a 3D extension to the improved centerline method. Invest Radiol 1997; 32:529-539.
38. Guttman MA, Prince JL, McVeigh ER. Tag and contour detection in tagged MR images of the left ventricle. IEEE TMI 1993; 13:74-88.
39. Moore CC, McVeigh ER, Zerhouni EA. Quantitative tagged magnetic resonance imaging of the normal human left ventricle. Topics in MRI 2000; 11:359-371.
40. Garot J, Bluemke DA, Osman NF, Rochitte ER, McVeigh ER, Zerhouni EA, Prince JL, Lima JA. Fast determination of regional myocardial strain fields from tagged cardiac images using harmonic phase MRI. Circulation 2000; 101:981-988.
41. Osman NF, McVeigh ER, Prince JL. Imaging heart motion using harmonic phase MRI. IEEE Trans Med Imag 2000; 19:186-202.
42. Jung B, Markl M, Föll D, Hennig J. Investigating myocardial motion by MRI using tissue phase mapping. Eur J Cardiothorac Surg. 2006;29 Suppl 1:S150-157.
43. Jung B, Föll D, Böttler P, Petersen S, Hennig J, Markl M. Detailed analysis of myocardial motion in volunteers and patients using high-temporal-resolution MR tissue phase mapping. J Magn Reson Imaging 2006 ;24:1033-1039.
44. Föll D, Jung B, Schilli E, Staehle F, Geibel A, Hennig J, Bode C, Markl M. Magnetic resonance tissue phase mapping of myocardial motion: new insight in age and gender. Circ Cardiovasc Imaging 2010;3:54-64.
45. Pelc NJ, Drangova M, Pelc LR, Zhu Y, Noll DC, Bowman BS, Herfkens RJ. Tracking of cyclic motion with phase-contrast cine MR velocity data. J Magn Reson Imag 1995; 5:339-345.
46. Hennig J, Schneider B, Peschl S, Markl M, Krause T, Laubenberger J. Analysis of myocardial motion based on velocity measurements with a black blood prepared segmented gradient-echo sequence: methodology and applications to normal volunteers and patients. J Magn Reson Imaging 1998; 8:868-877.
47. McInerney T, Terzopoulos D. A dynamic finite element surface model for segmentation and tracking in multidimensional medical images with application to cardiac 4D image analysis. Comput Med Imaging Graph 1995; 19:69-83.
48. Matsumura K, Nakase E, Haiyama T, Utsunomiya S. Automatic left ventricular volume measurements on contrast-enhanced utrafast cine magnetic resonance imaging. Eur J Radiol 1995; 20:126-132.
49. Goshtasby A, Turner DA. Segmentation of cardiac cine MR images for right and left ventricular chambers. IEEE Trans on Med Im 1995; 14:56-64.

50. Baldy C, Doueck P, Croisille P, Magnin IE, Revel D, Amiel M. Automated myocardial edge detection from breath-hold cine-MR images: evaluation of left ventricular volumes and mass. Magn Reson Imaging 1994; 12:589-598.
51. van der Geest RJ, Buller VGM, Jansen E, Lamb HJ, Baur LHB, van der Wall EE, de Roos A, Reiber JHC. Comparison between manual and automated analysis of left ventricular volume parameters from short axis MR images. J Comput Assist Tomogr 1997; 21:756-765.
52. Butler SP, McKay E, Paszkowski AL, Quinn R, Shnier RC, Donovan JT. Reproducibility study of left ventricular measurements with breath-hold cine MRI using a semiautomated volumetric image analysis program. J Magn Reson Imaging 1998; 8:467-472.
53. Kaushikkar SV, Li D, Haacke EM, Dávilla-Román VG. Addaptive bloodpool segmentation in three-dimensions: application to MR cardiac evaluation. J Magn Reson Imaging 1996; 6:690-697.
54. Singleton HR, Pohost GM. Automatic cardiac MR image segmentation using edge detection by tissue classification in pixel neighborhoods. Magn Reson Med 1997; 37:418-424.
55. Furber A, Balzer P, Cavaro-Menárd C, Croué A, Da Costa E, Lethimonnier F, Geslin P, Tadéi A, Jallet P, Le Jeune JJ. Experimental validation of an automated edge-detection method for a simultaneous determination of the endocardial and epicardial borders in short-axis cardiac MR images: application in normal volunteers. J Magn Reson Imaging 1998; 8:1006-1014.
56. Nachtomy E, RC, Vaturi M, Bosak E, Vered Z, Akselrod S. Automatic assessment of cardiac function from short-axis MRI: Procedure and clinical evaluation. Magn Reson Imag 1998; 16:365-376.
57. Lalande A, Legrand L, Walker PM, Guy F, Cottin Y, Roy S, Brunotte F. Automatic detection of left ventricular contours from cardiac cine magnetic resonance imaging using fuzzy logic. Invest Radiol 1999; 34:211-217.
58. Hautvast G, Lobregt S, Breeuwer M, Gerritsen F. Automatic Contour Propagation in Cine Cardiac Magnetic Resonance Images IEEE Trans Med Imag 2006;25:1472-1482.
59. Cocosco CA, Niessen WJ, Netsch T, et al. Automatic image-driven segmentation of the ventricles in cardiac cine MRI. J Magn Reson Imaging 2008; 28:366-374.
60. Codella NC, Weinsaft JW, Cham MD, Janik M, Prince MR, Wang Y. Left ventricle: automated segmentation by using myocardial effusion threshold reduction and intravoxel computation at MR imaging. Radiology 2008;248:1004-1012.
61. Lee HY, Codella N, Cham M, Prince M, Weinsaft J, Wang Y. Left ventricle segmentation using graph searching on intensity and gradient and a priori knowledge (lvGIGA) for short-axis cardiac magnetic resonance imaging. J Magn Reson Imaging. 2008;28:1393-1401.
62. Amini AA, Weymouth TE, Jain RC. Using dynamic programming for solving variational problems in vision. IEE Trans PAMI 1990; 12:855-867.
63. Angelié A, de Koning PJH, Danilouchkine M, van Assen HC, Koning G, van der Geest RJ, Reiber JHC. Optimizing the automated segmentation of the left ventricule in magnetic resonance images. Med Phys 2005; 32:1-7.
64. Pattynama PMT, Lamb HJ, van der Velde EA, van der Wall EE, de Roos A. Left ventricular measurements with cine and spin-echo MR imaging: a study of reproducibility with variance component analysis. Radiology 1993; 187:261-268.
65. Lamb HJ, Doornbos J, van der Velde EA, Kruit MC, Reiber JHC, de Roos A. Echo-panar MRI of the heart on a standard sytem: validation of measurement of left ventricular function and mass. J Comp Assist Tomogr 1996; 20:942-949.
66. Cootes TF, Beeston C, Edwards GJ, Taylor CJ. A unified framework for atlas matching using active appearance models. Proc Information Processing in Medical Imaging 1999, Lecture Notes in Computer Science 1999; 1613:322-333.

67. Mitchell SC, Lelieveldt BPF, van der Geest RJ, Bosch JG, Reiber JHC, Sonka M. Multistage hybrid active appearance model matching: Segmentation of left and right ventricles in cardiac MR images. IEEE Trans Med Imaging 2001; 20:415-423.
68. Mitchell SC, Lelieveldt BPF, van der Geest RJ, Bosch JG, Reiber JHC, Sonka M. Segmentation of cardiac MR images: An active appearance model approach. proc. SPIE Medical Imaging 2000 Image Processing 2000; 3979:224-234.
69. van der Geest RJ, Lelieveldt BPF, Angelié A, Danilouchkine M, Swingen C, Sonka M, Reiber JHC. Evaluation of a new method for automated detection of left ventricular boundaries in time series of magnetic resonance images using an Active Appearance Motion Model. J Cardiovasc Magn Reson 2004; 6:609-617.
70. van Assen HC, Danilouchkine MG, Frangi AF, Ordás S, Westenberg JJM, Reiber JHC, Lelieveldt BPF, SPASM: a 3D-ASM for Segmentation of Sparse and Arbitrarily Oriented Cardiac MRI Data, Med. Image Analysis 2006; 10:286-303.
71. Karwatowski SP, Brecker SJD, Yang GZ, Firmin DN, Sutton MStJ, Underwood SR. Mitral valve flow measured with cine MR velocity mapping in patients with ischemic heart disease: comparison with Doppler echocardiography. J Magn Res Imag 1995; 5:89-92.
72. Beerbaum P, Körperich P, Barth P, Esdorn H, Gieseke J, Meyer H. Noninvasive quantification of left-to-right shunt in pediatric patients. Phase-contrast cine magnetic resonance imaging compared with invasive oximetry. Circulation 103, 2476-2482. 2001.
73. Kondo C, Caputo GR, Semelka R, Foster E, Shimakawa A, Higgins CB. Right and left ventricular stroke volume measurements with velocity-encoded cine MR imaging: In vitro and in vivo validation. AJR 1991; 157:9-16.
74. de Roos A, Helbing WA, Niezen RA, Rebergen SA, van der Wall EE, Ottenkamp J. Magnetic resonance imaging in adult congenital heart disease. In: Higgins CB, Inwall JS, Pohost GM, editors. Current and future applications of magnetic resonance in cardiovascular disease. Armonk, NY: Futura Publishing Company, Inc, 1988: 163-172.
75. Powel AJ, Geva T. Blood flow measurement by magnetic resonance imaging in congenital heart disease. Pediatr Cardiol 2000; 21:47-58.
76. Rebergen SA, de Roos A. Congenital heart disease. Evaluation of anatomy and function by MRI. Herz. 2000;25:365-383.
77. Valente AM, Powell AJ. Clinical applications of cardiovascular magnetic resonance in congenital heart disease. Cardiol Clin. 2007;25:97-110.
78. van der Geest RJ, Niezen RA, van der Wall EE, de Roos A, Reiber JHC. Automated measurement of volume flow in the ascending aorta using MR velocity maps: evaluation of inter- and interobserver variability in healthy volunteers. J Comp Assist Tomogr 1998; 22:904-911.
79. Gerber BL, Raman SV, Nayak K, Epstein FH, Ferreira P, Axel L, Kraitchman DL. Myocardial first-pass perfusion cardiovascular magnetic resonance: history, theory, and current state of the art. J Cardiovasc Magn Reson. 2008;28;10:18.
80. Jerosch-Herold M, Swingen C, Seethamraju RT. Myocardial blood flow quantification with MRI by model-independent deconvolution. Med Phys 2002; 29:886-897.
81. Pack NA, DiBella EVR, Rust TC, Kadrmas DJ, McGann CJ, Butterfield R, Christian PE, Hoffman JM. Estimating myocardial perfusion from dynamic contrast-enhanced CMR with a model-independent deconvolution method. J Cardiovasc Magn Reson 2008;10:52.
82. Lee DC, Johnson NP. Quantification of absolute myocardial blood flow by magnetic resonance perfusion imaging. JACC Img 2009;2:761-770.
83. Al-Saadi N, Nagel E, Gross M, Bornstedt A, Schnackenburg B, Klein C, Klimek W, Oswald H, Fleck E. Noninvasive detection of myocardial ischemia from perfusion reserve based on cardiovascular Magnetic Resonance. Circulation 2000;101:1379-1383.

84. Nagel E, Klein C, Paetsch I, Hettwer S, Schnackenburg B, Wegscheider K, Fleck E. Magnetic resonance perfusion measurements for the noninvasive detection of coronary artery disease. Circulation 2003; 108:432-437.
85. Schwitter J, Wacker CM, van Rossum AC, Lombarid M, Al-Saadi N, Ahlstrom H, Dill T, Larsson HBW, Flamm SD, Marquard M, Johansson L. MR-IMPACT: comparison of perfusion-cardiac magnetic resonance with single-photon emission computed tomography for the detection of coronary artery disease in a multicentre, multivendor, randomized trial. Eur Heart J 2008; 29:480-489.
86. Bidaut LM, Vallee JP. Automated registration of dynamic MR images for the quantification of myocardial perfusion. J Magn Reson Imaging 2001;13:648-655.
87. Adluru G, DiBella EVR, Schabel MC., Model-Based Registration for Dynamic Cardiac Perfusion MRI. J Magn Reson Imag. 2006;24:1062–1070.
88. Adluru G, DiBella EV, Schabel MC. Model-based registration for dynamic cardiac perfusion MRI. J Magn Reson Imaging. 2006;24:1062-1070.
89. Milles J, van der Geest RJ, Jerosch-Herold M, Reiber JH, Lelieveldt BPF. Fully automated motion correction in first-pass myocardial perfusion MR image sequences. IEEE Trans Med Imaging. 2008;27:1611-1621.
90. Kim RJ, Fieno DS, Parrish TH, Harris K, Chen EL, Simonetti O, Bundy J, Finn JP, Klocke FJ, Judd RM. Relationship of MRI delayed contrast enhancement to irreversible injury, infarct age, and contractile function. Circulation 1999; 100:1992-2002.
91. Kim RJ, Wu E, Rafael A, Chen EL, Parker MA, Simonetti O, Klocke FJ, Bonow RO, Judd RM. The use of contrast-enhanced magnetic resonance imaging to identify reversible myocardial dysfunction. New J Med 2000; 343:1445-1453.
92. Oshinski JN, Yang ZQ, Jones JR, Mata JF, French BA. Imaging time after Gd-DTPA injection is critical in using delayed enhancement to determine infarct size accurately with magnetic resonance imaging. Circulation 2001; 104:2838-2842.
93. Bondarenko O, Beek AM, Hofman MB, Kühl HP, Twisk JW, van Dockum WG, Visser CA, van Rossum AC. Standardizing the definition of hyperenhancement in the quantitative assessment of infarct size and myocardial viability using delayed contrast-enhanced CMR. J Cardiovasc Magn Reson. 2005; 7(2):481-485.
94. Beek AM, Bondarenko O, Afsharzada F, van Rossum AC. Quantification of late gadolinium enhanced CMR in viability assessment in chronic ischemic heart disease: a comparison to functional outcome. J Cardiovasc Magn Reson 2009;11:6
95. Schuijf JD, Kaandorp TA, Lamb HJ, van der Geest RJ, Viergever EP, van der Wall EE, de Roos A, Bax JJ. Quantification of myocardial infarct size and transmurality by contrast-enhanced magnetic resonance imaging in men. Am J Cardiol 2005; 94:284-288.
96. Amado LC, Gerber BL, Gupta VK, Rettmann DW, Szarf G, hock R, sir Kraitchman DL, ma JA. Accurate and objective infarct sizing by contrast-enhanced magnetic resonance imaging in a canine myocardial infacrtion model. J Am Coll Cardiol 2004; 44:2383-2389.
97. Hsu LY, Natanzon A, Kellman P, Hirsch GA, Aletras AH, Arai AE. Quantitative Myocardial Infarction on Delayed Enhancement MRI. Part I: Animal Validation of an Automated Feature Analysis and Combined Thresholding Infarct Sizing Algorithm. J Cardiovasc Magn Reson 2006;23:298–308.
98. Hennemuth, Seeger A, Friman O, Miller S, Klumpp B, Oeltze S, Peitgen HO. A comprehensive approach to the analysis of contrast enhanced cardiac MR images. Trans Med Imag 2008;27:1592-1610